Electronic Supplementary Information

Preparation of intrinsically fragile bent crystals

Tomohiro Seki,*[a] Shiori Kobayashi,[a] Rintaro Ishikawa,[a] Keigo Yano,[b] Takumi Matsuo,[b,c] and Shotaro Hayashi[b,c]

[a] Department of Chemistry, Faculty of Science, Shizuoka University, Shizuoka City, Shizuoka 422-8529, Japan
E-mail: seki.tomohiro@shizuoka.ac.jp
[b] School of Engineering Science, Kochi University of Technology, 185 Miyanokuchi, Tosayamada, Kami, Kochi 782-8502, Japan
[c] Research Institute, Kochi University of Technology, 185 Miyanokuchi, Tosayamada, Kami, Kochi 782-8502, Japan

Email: seki.tomohiro@shizuoka.ac.jp

Contents

1. General

All commercially available reagents and solvents are of reagent grade and were used without further purification unless otherwise noted. Solvents for the synthesis were purchased from commercial suppliers, degassed by three freeze-pump-thaw cycles and further dried over molecular sieves (4 Å). Purification by column chromatography was performed with a silica gel 60N (spherical, neutral, 40–100 μm mesh, Kanto chemicals, Japan). NMR spectra were recorded on a JEOL ECA-600 spectrometer (^{1}H: 600 MHz; ^{13}C: 151 MHz) using tetramethylsilane and $CDCl_3$ as internal standards, respectively. UV-vis absorption spectra were recorded on a JASCO V-750 spectrometer. The absorption spectra of the solid samples were recorded on a JASCO V-750 spectrophotometer equipped with JASCO ISV-922 integrating sphere. Emission spectra were recorded on a JASCO FP-8600 spectrometer. Luminescence microscopic spectra were recorded on a Photonic Hamamatsu PMA-12 Multichannel Analyzer (C14631-01). A cooling/heating stage on JHC 10002L was used for temperature changes of solid samples. The emission quantum yields of the solid samples were recorded on a JASCO ILF-835 integrating sphere that was interfaced with a JASCO FP-8600 spectrofluorometer. Emission lifetime measurements were recorded on a Hamamatsu Quantaurus-Tau spectrometer. High resolution mass spectra were recorded on a Thermo Scientific Exactive at the Center for analytical instrumentation at Chiba University. Photographs were obtained using Olympus BX53, SZX10, or Leica M205c microscopes with Sony α7S, Olympus DP74, or Leica Flexacam C3 digital cameras, respectively. Differential scanning calorimetry (DSC) measurements were recorded on a Shimadzu DSC60 instrument using Al_2O_3 as a reference material. Powder XRD data were recorded on a Rigaku SmartLab diffractometer or MiniFlex600 with Cu-K_α radiation with a monochrometer.

Single crystal X-ray diffraction analyses: A suitable crystal was mounted with Paratone oil on a MiTeGen MicroMounts and transferred to the Four-circle Kappa Geometry Goniometer of a RIGAKU XtaLAB Synergy-S or R/Si system with 1.2 kW PhotonJet-S microfocus rotating anode using graphite monochromated Cu-K_a radiation and HyPix-6000HE detector. Cell parameters were determined and refined, and raw frame data were integrated using CrysAlis^{Pro} (Agilent Technologies). The structures were solved by direct methods with (SHELXT)[S1] and refined by full-matrix least-squares techniques against F^2 (SHELXL-2018/3)[S2] by using Olex2 software package.[S3] The intensities were corrected for Lorentz and polarization effects. The non-hydrogen atoms were refined anisotropically. Hydrogen atoms were placed using AFIX instructions. Simulated powder patterns were generated with Mercury software[S4] from the structures determined by single-crystal diffraction analyses.

2. Synthesis

*Synthesis of **1a***[S5]

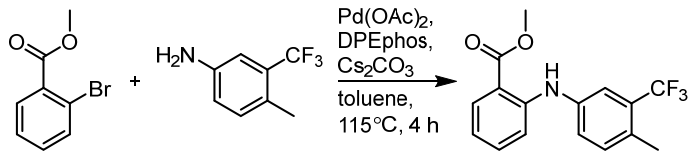

1a

An oven-dried two-neck flask was connected to a vacuum/argon manifold through a rubber tube. It was evacuated and then backfilled with argon. This cycle was repeated three times. To this flask, methyl 2-bromobenzoate (430 mg, 2.0 mmol), 4-methyl-3-(trifluoromethyl)aniline (351 mg, 2.0 mmol), palladium(II) acetate (10.7 mg, 4.8×10^{-2} mmol), bis[2-(diphenylphosphino)phenyl] ether (DPEphos) (31.7 mg, 5.9×10^{-2} mmol), cesium carbonate (918 mg, 2.8 mmol) were added and dissolved in toluene (2.7 mL). The mixture was stirred at 115°C for 4 h. After the reaction completion was monitored by TLC analysis, the mixture was cooled to room temperature, and the reaction was quenched by the addition of ca. 20 mL of ethyl acetate. The solution was washed with 2 M HCl (6.8 mL), ethyl acetate, and brine. The combined organic layers were dried over $MgSO_4$ and then evaporated in vacuo. The residue was purified by column chromatography on silica gel (CH_2Cl_2/hexane = 1:2) and obtained **1a** as a white powder (592 mg, 1.9 mmol, 96%).

^{1}H NMR (600 MHz, $CDCl_3$, δ): 2.45 (s, 3H), 3.91 (s, 3H), 6.77 (t, J = 7.6 Hz, 1H), 7.17 (d, J = 8.9 Hz, 1H), 7.24 (d, J = 8.3 Hz, 1H), 7.30 (d, J = 7.9 Hz, 1H), 7.34 (t, J = 7.7 Hz, 1H), 7.48 (s, 1H), 7.98 (d, J = 7.9 Hz, 1H), 9.49 (s, 1H). The synthesis of **1a** has already been reported,[S5] and our ^{1}H NMR spectrum is matched with the previously reported spectrum.

*Synthesis of **1***[S5]

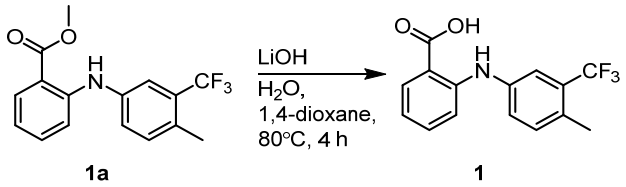

To a two-neck flask, **1a** (463 mg, 1.5 mmol, 1.0 equiv) was added and dissolved in 1,4-dioxane (7.5 mL) and 1 mL of an aqueous solution of LiOH (180 mg, 7.5 mmol) was added. After the mixture was stirred at 80°C for 4 h, the reaction completion was monitored by TLC analysis. The mixture was cooled to room temperature and the reaction was quenched by the addition of 15 mL of HCl aqueous solution (0.5 M). After the addition of ethyl acetate, the mixture was washed with water and brine and extracted with ethyl acetate. The combined organic layers were dried over Na_2SO_4 and then evaporated in vacuo to give analytically pure **1** (404 mg, 1.37 mmol, 91%).

^{1}H NMR (600 MHz, DMSO-d_6, δ): 2.40 (s, 3H), 6.84 (t, J = 7.6 Hz, 1H). 7.20 (d, J = 8.3 Hz, 1H), 7.42 (m, 3H), 7.48 (s, 1H), 7.91 (d, 1H), 9.63 (br s, 1H), 13.2 (s, H). ^{13}C NMR (151 MHz, $CDCl_3$, δ): 18.9 (*C*H$_3$), 110.8 (*C*), 113.9 (*C*H), 117.8 (*C*H), 120.7 (*C*H), 124.3 (*C*, d, J = 274.5 Hz), 125.2 (*C*H), 130.0 (*C*, q, J = 30.3 Hz), 132.1 (*C*H), 133.1 (*C*H), 135.5 (*C*H), 138.4 (*C*), 148.6 (*C*), 173.9 (*C*). The synthesis of **1** has already been reported,[S5] and our ^{1}H NMR spectrum is matched with the previously reported spectrum. Our ^{13}C NMR spectrum of **1** is slightly different from the previously reported one.[S5] It should be noted that two expected carbon signals of **1** are not detected in the previous ^{13}C NMR spectrum of **1** out of 15 carbon signals as judged from the structure of **1**. MS-ESI (m/z): $[M+H]^+$ calcd for $C_{17}H_{10}N$, 296.0893; found, 296.0887.

3. Mechanical properties

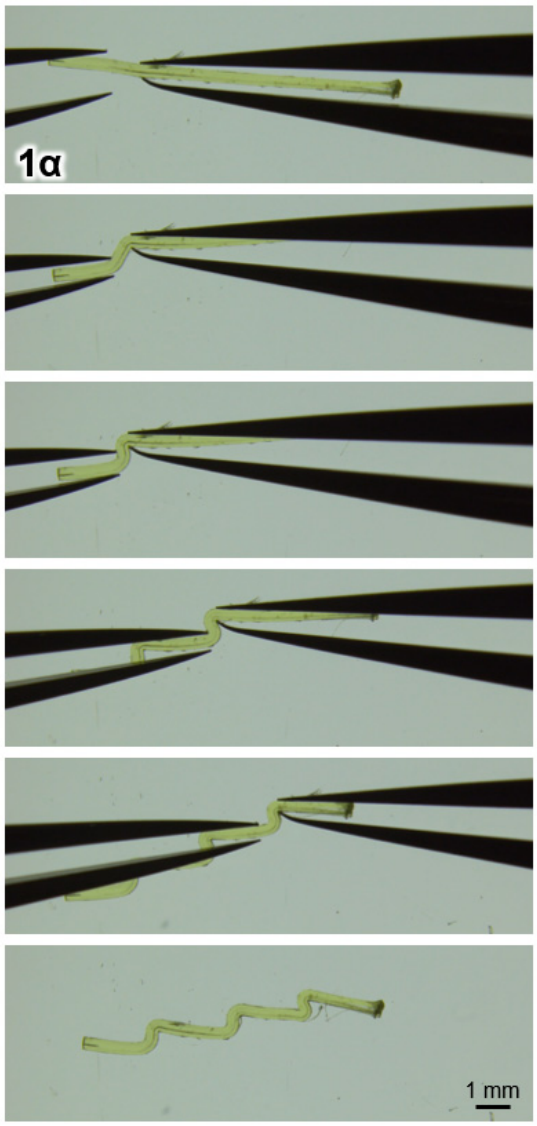

Fig. S1 Photographs of a **1α** crystal upon applying mechanical stimulation. These photographs are derived from the Supporting Movie S1.

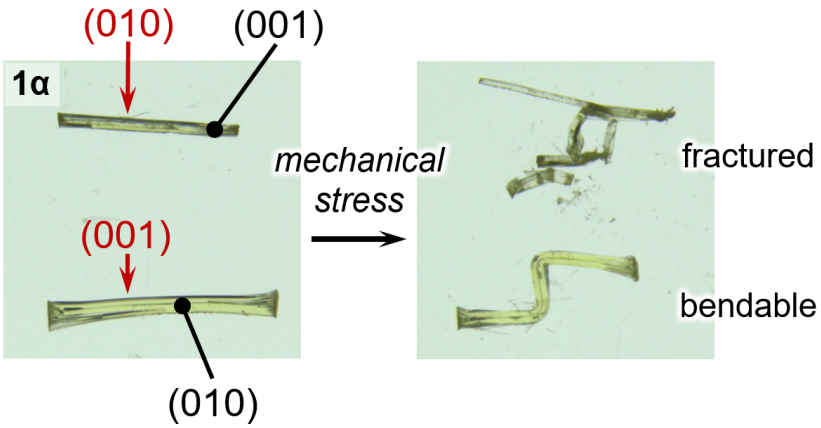

Fig. S2 Photographs of two pieces of crystal of **1α** upon pushing on (010) and (001) planes (the upper and bottom crystals, respectively).

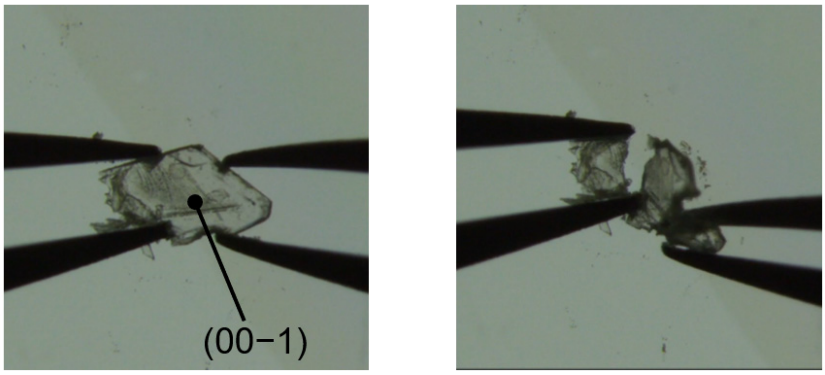

Fig. S3 Photographs of a crystal of **1β** upon applying mechanical force to the side faces rather than the main face (00-1), resulting in the fluctuation.

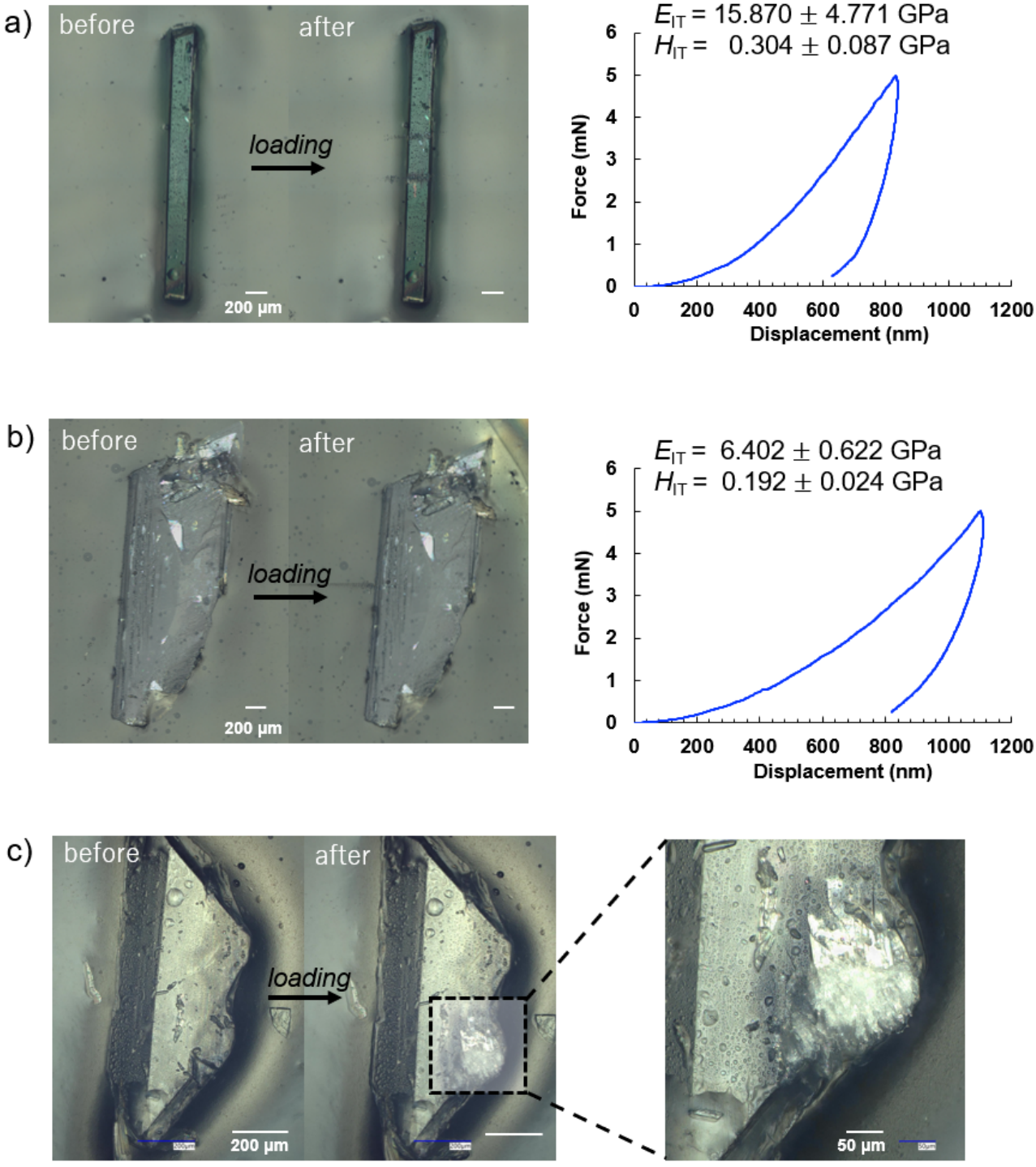

Fig. S4 Nanoindentation test of the crystals of **1**. Left: Microscope images of a) **1α**, b) **1β**, and c) **1γ** before and after loading. Right: Nanoindentation curve with elasticity, *E*, and hardness, *H* of a) **1α** and b) **1β**.

Note: For **1γ**, the crystal shape had many inclinations, so the indenter could not be pressed vertically, and the nanoindentation curve could not be obtained.

4. Crystal structure analyses

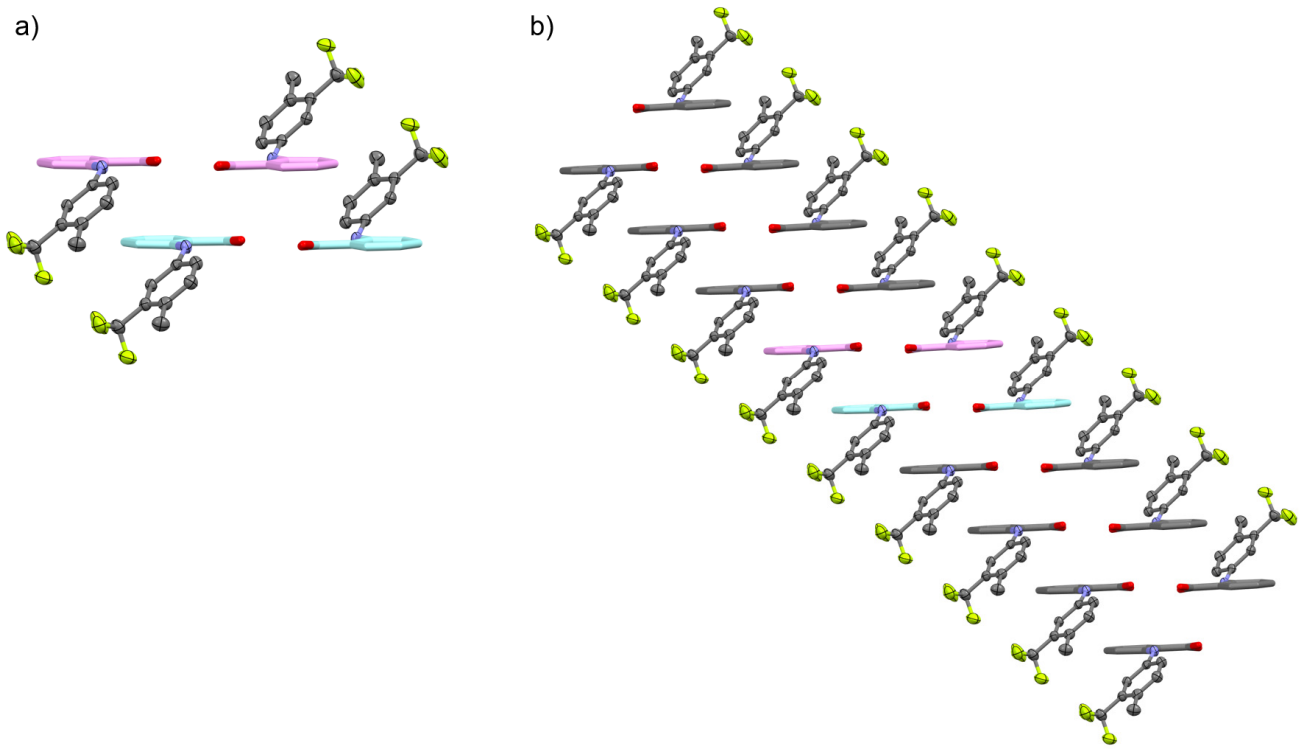

Fig. S5 Single-crystal structure of **1α**.

Table S1 Summary of X-ray crystallographic data of **1α**, **1β**, and **1γ**.

crystal	**1α**	**1β**	**1γ**
CCDC Number	2350732	2350733	2350734
Empirical Formula	$C_{15}H_{12}F_3NO_2$	$C_{15}H_{12}F_3NO_2$	$C_{15}H_{12}F_3NO_2$
Formula Weight	295.26	295.26	295.26
Crystal System	orthorhombic	triclinic	monoclinic
Space group	$Pna2_1$	P-1	$P2_1/n$
Crystal Size / mm	0.9×0.09×0.02	0.50×0.33×0.10	0.3 × 0.04 × 0.02
a / Å	12.3091(2)	6.6355(5)	4.9586(2)
b / Å	5.07340(10)	7.3234(5)	11.2709(4)
c / Å	41.7053(4)	15.7183(10)	24.1190(8)
α / °	90	82.822(5)	90
β / °	90	80.835(6)	95.674(3)
γ / °	90	65.136(7)	90
V / Å^3	2604.45(7)	682.74(9)	1341.36(8)
Z value	8	2	4
D_{calc} / g cm^{-3}	1.506	1.436	1.462
Temperature / K	173.00(10)	173.00(10)	173.00(10)
$2\theta_{max}$ / °	155.442	152.954	154.588
μ(Cu K$_\alpha$) / mm^{-1}	1.115	1.064	1.083
No. of Reflections	45890	6755	8206
R_1[a]	0.0406	0.0614	0.0482
wR_2[b]	0.1087	0.1873	0.1359
GOF	1.072	1.084	1.067
Max./Mini. peak I[d] / Å^3	0.26/−0.31	0.27/−0.38	0.34/−0.31

[a]: $I > 2.00\sigma(I)$. [b]: All reflections. [c]: Goodness of Fit Indicator. [d]: in Final Diff. Map.

***Energy framework calculations*:** Structures were taken from the single-crustal structures for the calculations without optimization. For the energy framework calculations, CrystalExplorer 21 was used to visualize the pairwise interaction energies (B3LYP/6-31G (d,p), Gaussian09 program). The calculated total energy components consist of electrostatic, polarization, dispersion, and exchange repulsion energies. Energy frameworks were drawn at the tube size of 60 and the cut-off value of 5 kJ mol^{-1}.

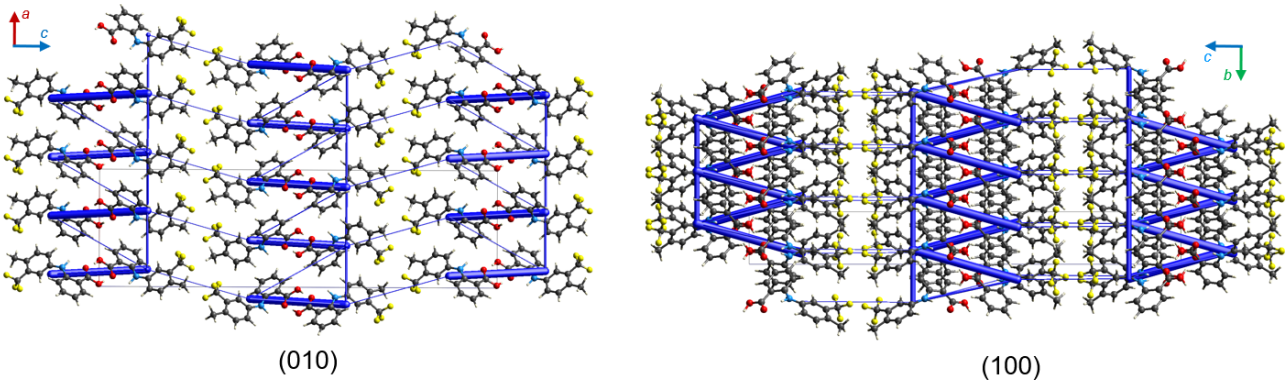

Fig. S6 Energy framework of **1α** representing the total interaction energy (blue cylinders).

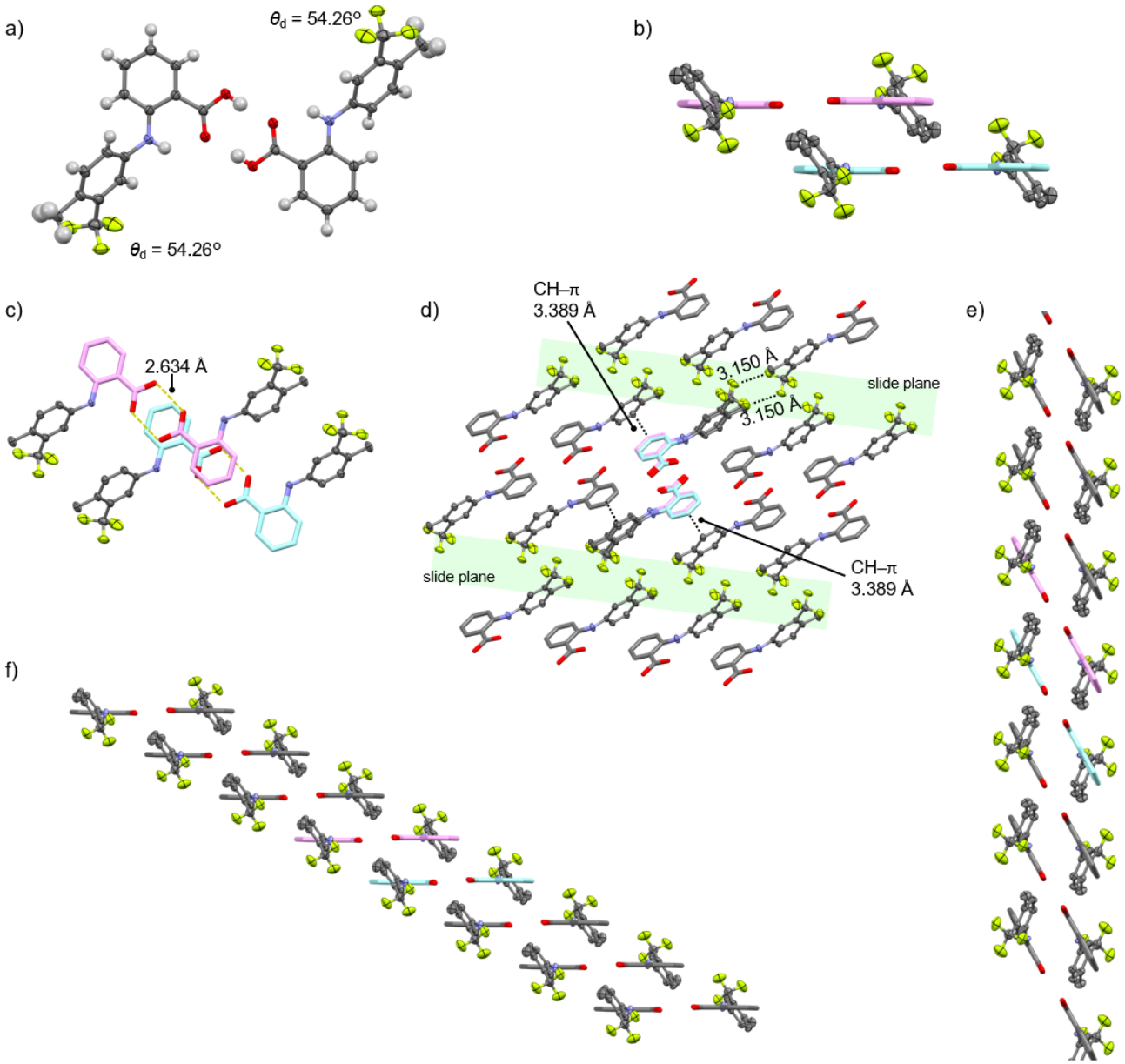

Fig. S7 Single-crystal structure of **1β**.

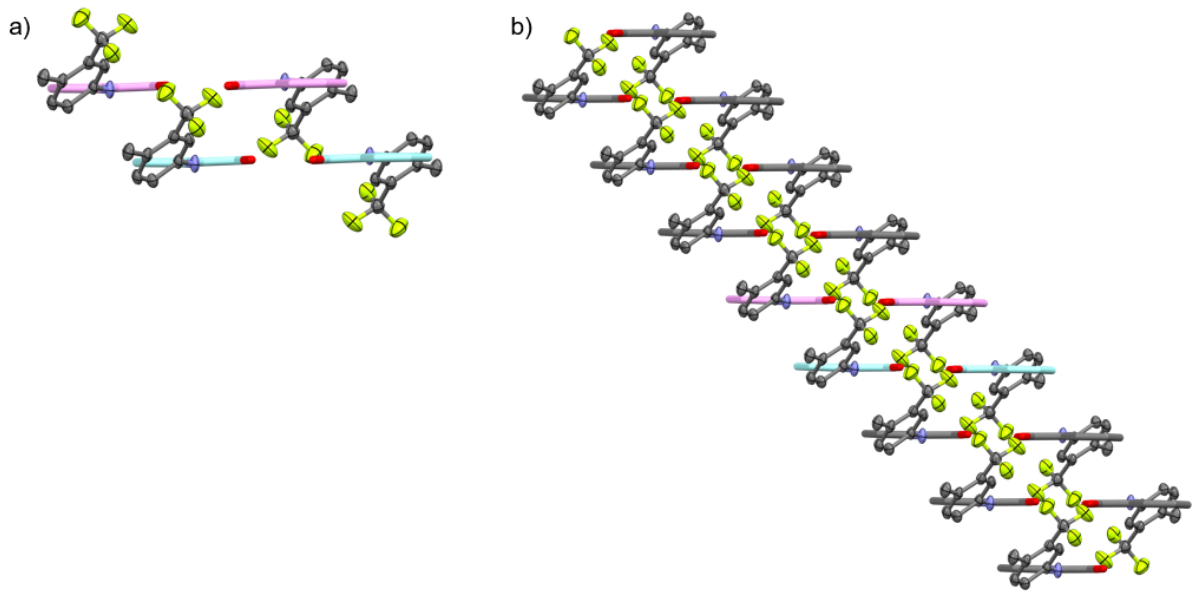

Fig. S8 Single-crystal structure of **1γ**

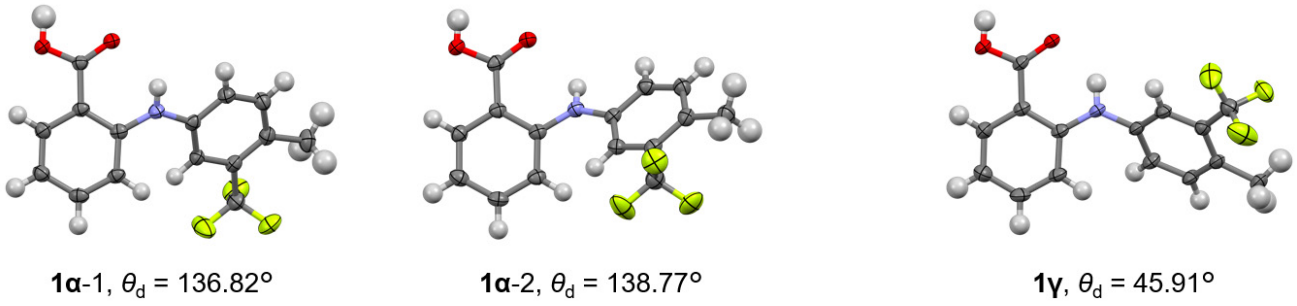

Fig. S9 Single-crystal structure of **1α** and **1γ** showing different θ_d values.

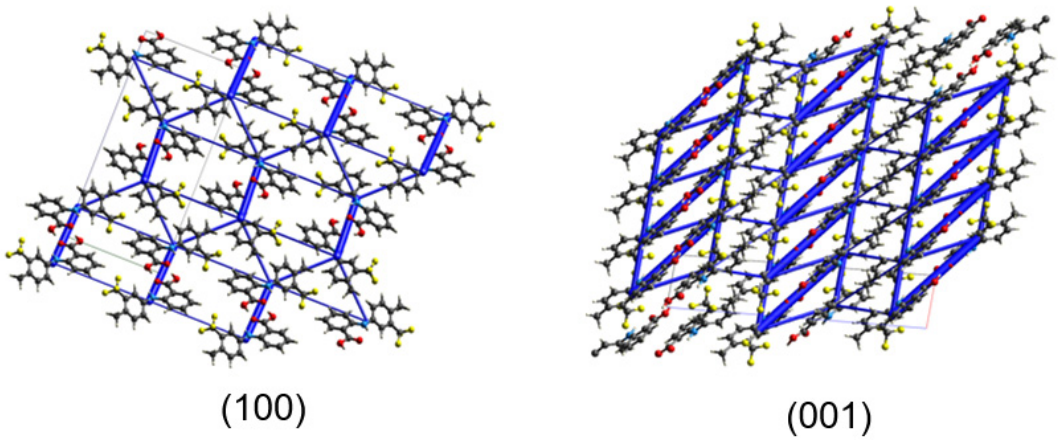

Fig. S10 Energy framework of **1γ** representing the total interaction energy (blue cylinders).

5. Photophysical properties

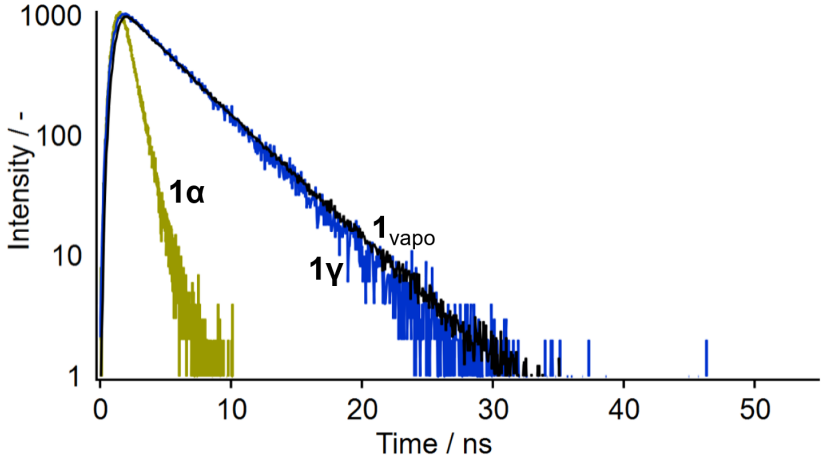

Fig. S11 Emission decay profiles of **1α** (yellow line), **1γ** (blue line), and **1**$_{vapo}$ (black line). Excitation wavelength: 365 nm. Monitoring emission wavelengths of **1α**, **1γ**, and **1**$_{vapo}$ are 469, 437, and 442 nm, respectively.

Table S2 Photophysical properties of **1**

	Φ_{em} / %[a]	τ_{av} / ns [a,b,c]	τ_1 / ns (A / -)	τ_2 / ns (A / -)	k_r[d] / s^{-1}	k_{nr}[e] / s^{-1}
1α	5.6	0.66	0.33 (0.20)	0.75 (0.80)	8.5×10^7	1.4×10^9
1γ	51	3.9	3.9 (1)	-	1.3×10^8	1.3×10^8
1$_{vapo}$	46	4.2	2.8 (0.23)	4.4 (0.77)	1.1×10^8	1.3×10^8

[a]: λ_{ex} = 365 nm. [b]: λ_{em} of **1α** = 469 nm, λ_{em} of **1γ** = 437 nm, λ_{em} of **1**$_{vapo}$ = 442 nm. [c]: $\tau_{av} = \Sigma\tau_n^2 A_n / \Sigma\tau_n A_n$. [d]: Radiative rate constants (k_r) were estimated from the equation $k_r = \Phi_{em}/\tau_{av}$. [e]: Nonradiative rate constants (k_{nr}) were estimated from the equation $k_{nr} = k_r(1 - \Phi_{em})\Phi_{em}$.

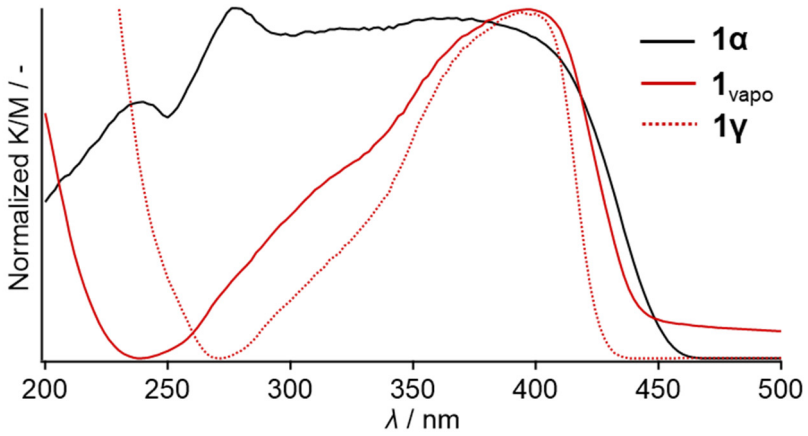

Fig. S12 Normalized absorption spectra of the solid sample of **1α**, **1γ**, and **1**$_{vapo}$ based on the diffuse reflection spectra.

***DFT calculations*:** All calculations were performed using the Gaussian 09W (revision C.01) and Gaussian 09 program packages.[S6] In the calculations, the 6-31+G(d) basis set and B3LYP functionals were used. A monomer structure of **1** was obtained by the optimization in the gas phase before TD-DFT calculations. The geometry of the dimeric structures of **1α** and **1γ** were calculated using coordinates of heavy atoms taken from the single-crystal structure. The positions of heavy atoms were fixed and only the positions of H atoms were optimized using the Spartan'20[S7] MMFF force-field calculations before TD-DFT calculations. Molecular orbitals were drawn using GaussView 6.1.1.

Calculated energies between HOMO and LUMO of monomer **1**, dimers **1α**, and **1γ** are 309 nm (4.01 eV), 322 nm (3.84 eV), and 311 nm (3.99 eV). The relative orders of these calculated energies are in line with the experimental results: the $\lambda_{em,max}$ of monomer **1**, **1α**, and **1γ** are 424, 469, and 437 nm (Fig. S13), pointing out the validity of the calculation conditions. Considering their orbitals upon transition from HOMO to LUMO (Fig. S14), monomer **1** and **1γ** have similar characteristics. The HOMO of monomer **1** spreads over the entire molecule, while their LUMO is mainly located on the benzoic acid group. For **1γ**, molecule **1γ**-1 has the HOMO and LUMO similar to those of monomer **1**. The orbital located on the benzoic acid moiety of molecule **1γ**-2 indicates a slight increase of the intermolecular character for the HOMO–LUMO transition of **1γ** compared to monomer **1**. Contrary, the HOMO–LUMO transition of **1α** has more exclusively intermolecular character from the entire molecule of **1α**-2 (HOMO) to the benzoic acid moiety of **1α**-1 (LUMO). Such intermolecular charge transfer character of the excited state of **1α** should cause the experimentally observed longer $\lambda_{em,max}$ of **1α**.

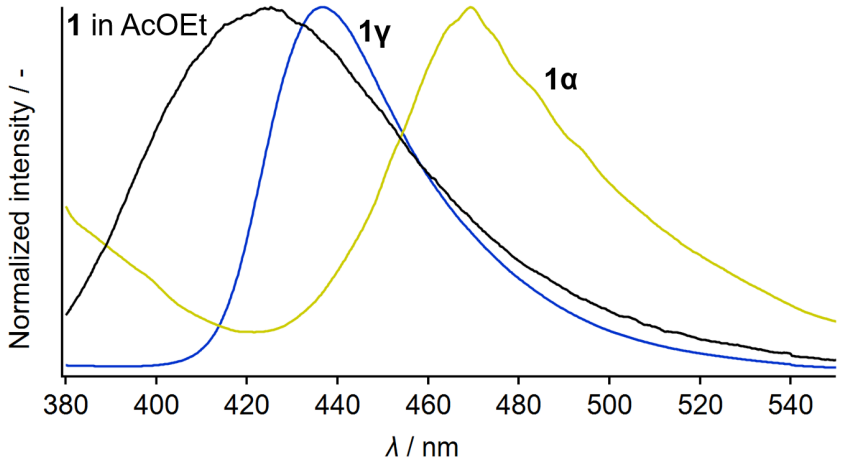

Fig. S13 Emission spectra of **1α**, **1γ**, and monomer **1** in ethyl acetate (c = 10 μM). Excitation wavelength is 365 nm for **1α** and **1γ** and 289 nm for monomer **1**.

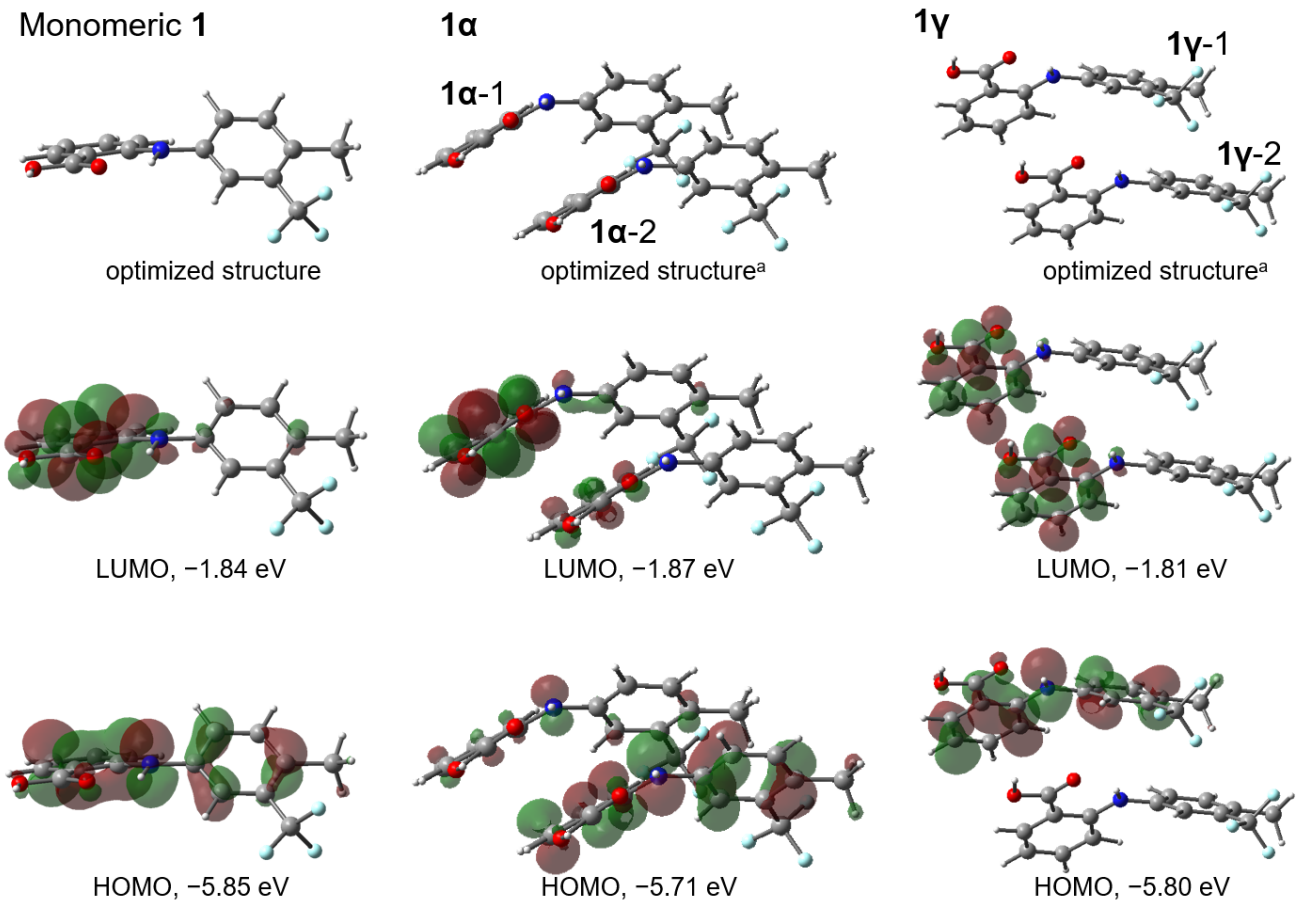

Fig. S14 Energy levels and frontier orbitals of HOMO and LUMO of monomer **1**, **1α**, and **1γ**.
[a]: The optimized structures of **1α** and **1γ** are derived from the single crystal structure and only H atom positions are optimized before TD-DFT calculations.

6. Phase transitions of the unbent crystals

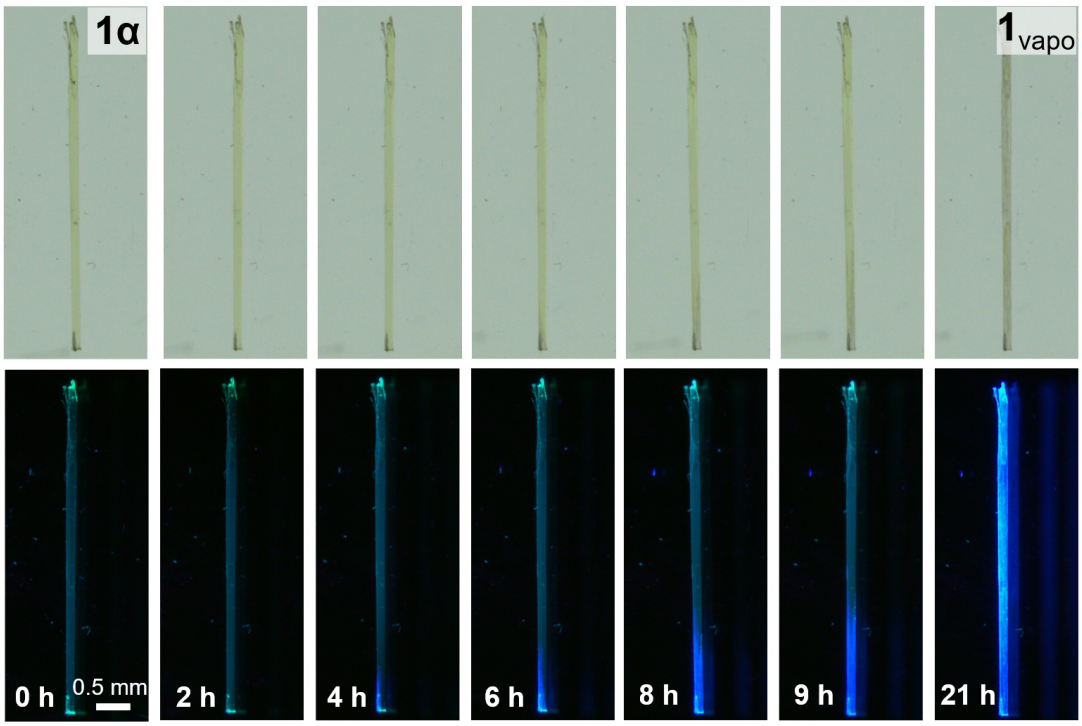

Fig. S15 Photographs of a crystal of **1α** upon exposure to ethyl acetate to give $\mathbf{1}_{vapo}$ recorded under ambient (top) and UV light (bottom).

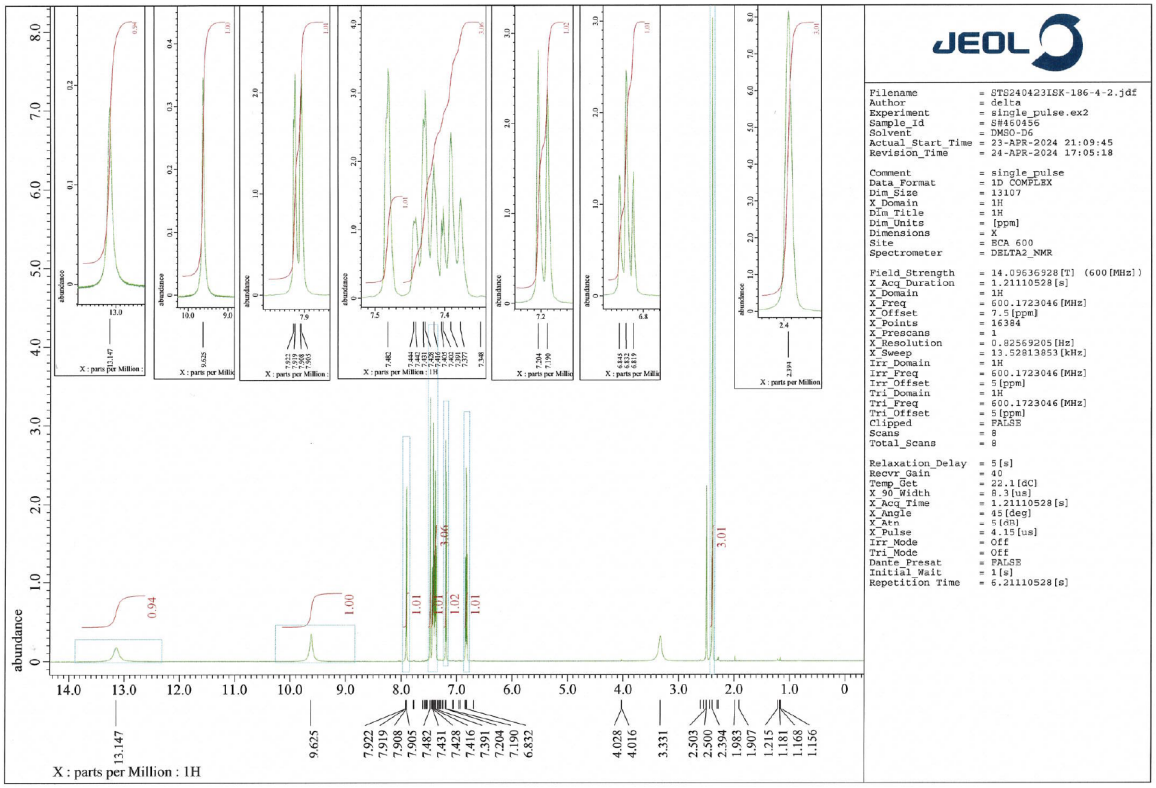

Fig. S16 ^{1}H NMR spectrum of $\mathbf{1}_{vapo}$ in DMSO-d_6.

Table S3 Summary of X-ray crystallographic data of $\mathbf{1}_{vapo}$ and bent $\mathbf{1}_{vapo}$.

crystal	**1α**[e]	$\mathbf{1}_{vapo}$[f]	bent $\mathbf{1}_{vapo}$[g]	**1γ**[e]
CCDC Number	2350732	-[h]	-[h]	2350734
Empirical Formula	$C_{15}H_{12}F_3NO_2$	$C_{15}H_{12}F_3NO_2$	$C_{15}H_{12}F_3NO_2$	$C_{15}H_{12}F_3NO_2$
Formula Weight	295.26	295.26	295.26	295.26
Crystal System	orthorhombic	monoclinic	monoclinic	monoclinic
Crystal Size / mm	0.9×0.09×0.02	0.11×0.02×0.02	0.81×0.1×0.02	0.3×0.04×0.02
a / Å	12.3091(2)	4.9656(2)	4.95200(10)	4.9586(2)
b / Å	5.07340(10)	11.2508(4)	11.2721(2)	11.2709(4)
c / Å	41.7053(4)	24.1225(13)	24.0986(5)	24.1190(8)
α / °	90	90	90	90
β / °	90	95.594(4)	95.742(2)	95.674(3)
γ / °	90	90	90	90
V / Å^3	2604.45(7)	1341.23(10)	1338.42(5)	1341.36(8)
Space group	$Pna2_1$	$P2_1/n$	$P2_1/n$	$P2_1/n$
Z value	8	4	4	4
D_{calc} / g cm^{-3}	1.506	1.462	1.465	1.462
Temperature / K	173.00(10)	173.00(10)	173.00(10)	173.00(10)
$2\theta_{max}$ / °	155.442	154.572	155	154.588
μ(Cu K$_\alpha$) / mm^{-1}	1.115	1.083	1.085	1.083
No. of Reflections	45890	24844	23566	8206
R_1[a]	0.0422	0.0786	0.0607	0.0547
wR_2[b]	0.1087	0.1743	0.1462	0.1359
GOF	1.072	1.085	1.056	1.067
Max./Mini. peak *I*[d] / Å^3	0.26/−0.31	0.31/−0.27	0.32/−0.29	0.34/−0.31

[a]: $I > 2.00\sigma(I)$. [b]: All reflections. [c]: Goodness of Fit Indicator. [d]: in Final Diff. Map. [e]: Data of **1α** and **1γ** are for the references and the same data are shown in Table S1. [f]: A $\mathbf{1}_{vapo}$ crystal was prepared from pristine **1α** by exposure to ethyl acetate. The crystal was cut into a small piece for the single-crystal XRD measurement. [g]: A bent $\mathbf{1}_{vapo}$ crystal was prepared from a mechanically bent **1α** crystal by exposure to ethyl acetate. The crystal was cut into a small piece for the single-crystal XRD measurement. [h]: These CIF data are not deposited to the CCDC database because essentially the same as that of **1γ**.

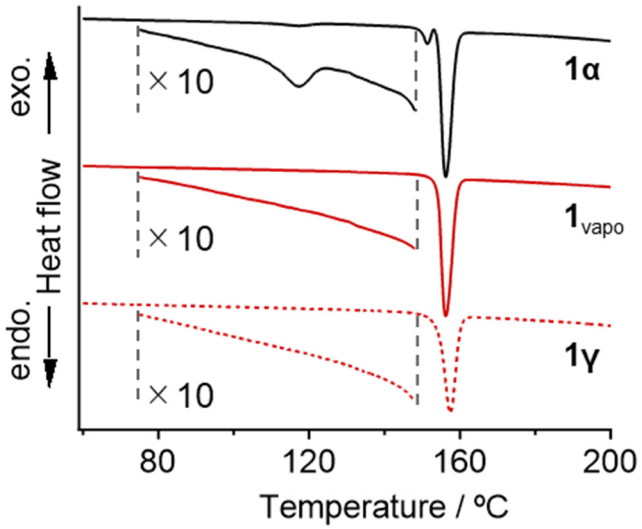

Fig. S17 DSC traces of **1α**, **1γ**, and **1**$_{vapo}$ with a heating rate of 5°C/min.

Note 1: The DSC traces of **1α**, **1γ**, and **1**$_{vapo}$ all have intense peaks at ca. 160°C assignable to melt. A DSC trace of **1α** has two small peaks (117 and 151°C) before the melting point. Contrary, the DSC traces of **1γ** and **1**$_{vapo}$ are featureless and similar to each other. This supports that **1γ** and **1**$_{vapo}$ are the same molecular arrangements. This is in line with the spectroscopic (Fig. 6b), the XRD data (Table S3), and the mechanical properties (Fig. 6c) of **1γ** and **1**$_{vapo}$.

Note 2: For the several small peaks of the DSC trace of **1α** can not be clearly assigned owing to the slow thermal phase transition. However, in the different heating experiments (constant temperature of 110°C for ~10 h), the thermal phase transition of **1α** to **1γ** was demonstrated (see Fig. S20).

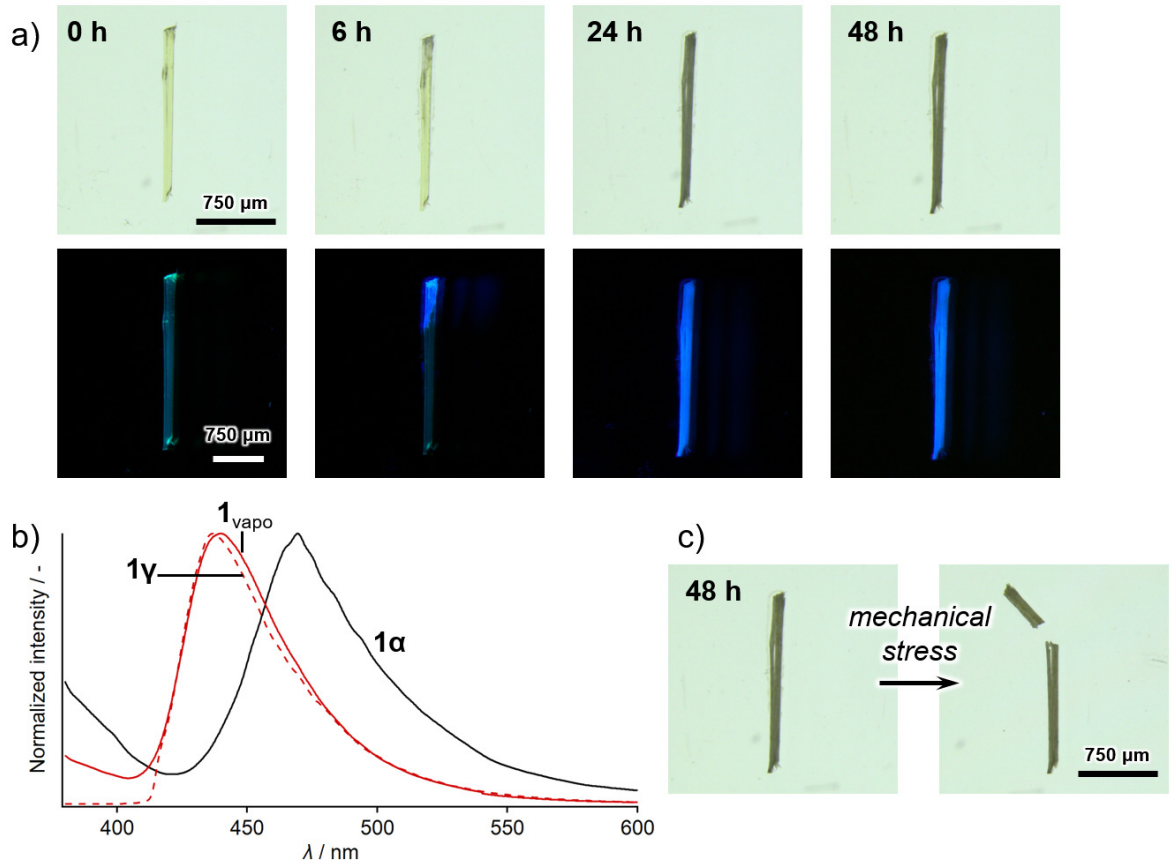

Fig. S18 a) Photographs of **1α** upon exposure to acetone vapor to form $\mathbf{1}_{vapo}$ under room (left) and UV light (right). b) Luminescence microscopic spectra of a piece of crystal of **1α**, **1γ**, and $\mathbf{1}_{vapo}$ under excitation at 365 nm. c) Photographs of a crystal of **1α** upon the addition of mechanical force, confirming the brittle nature of the resulting crystal $\mathbf{1}_{vapo}$.

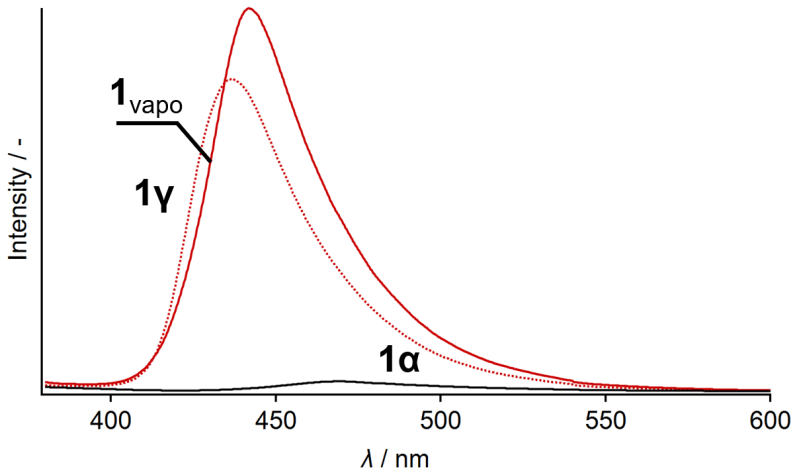

Fig. S19 Luminescence microscopic spectra of a piece of crystal of **1α**, **1γ**, and $\mathbf{1}_{vapo}$ under excitation at 365 nm.

Note: These emission spectra are not normalized, indicating the remarkable increase in the emission intensity.

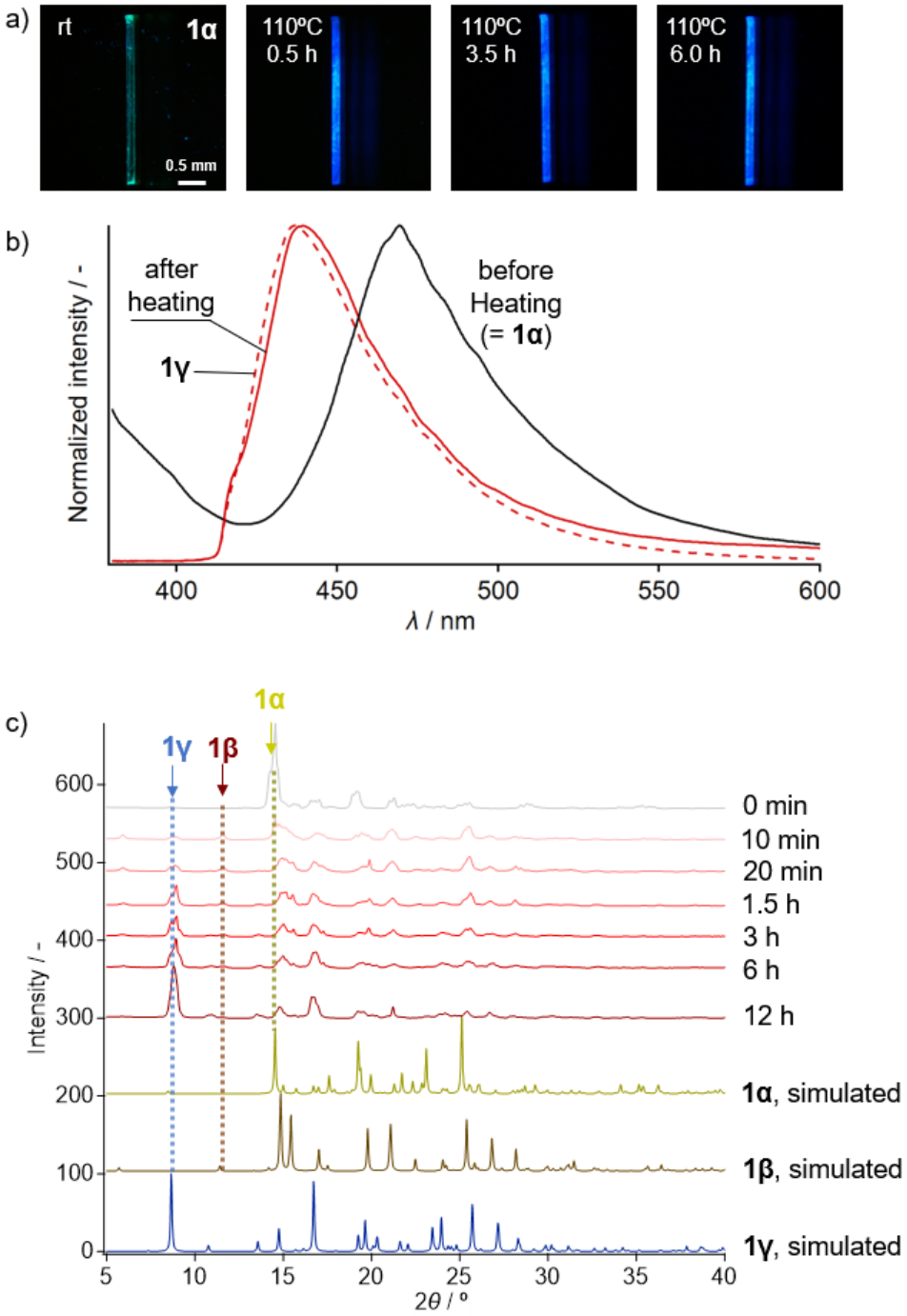

Fig. S20 a) Photographs of a piece of crystal of **1α** upon heating at 110°C taken under UV light. b) Luminescence microscopic spectra of **1α** before and after heating and **1γ** (for the reference) under excitation at 365 nm. c) Changes of powder XRD patterns of **1α** upon heating at 110°C and simulated powder patterns of **1α**, **1β**, and **1γ** derived from the single-crystal structures for references. Typical diffraction peaks of each polymorph are denoted by allows.

Note: The powder XRD data (Fig. S20c) implied the stepwise phase transitions from **1α** to **1β** and then to **1γ**. These sequential phase transitions are relatively slow (typically >12 h). The crystal obtained after heating for 12 h showed an emission spectrum similar to that of pristine **1γ** (Fig. S20b).

7. Phase transition of the bent crystals

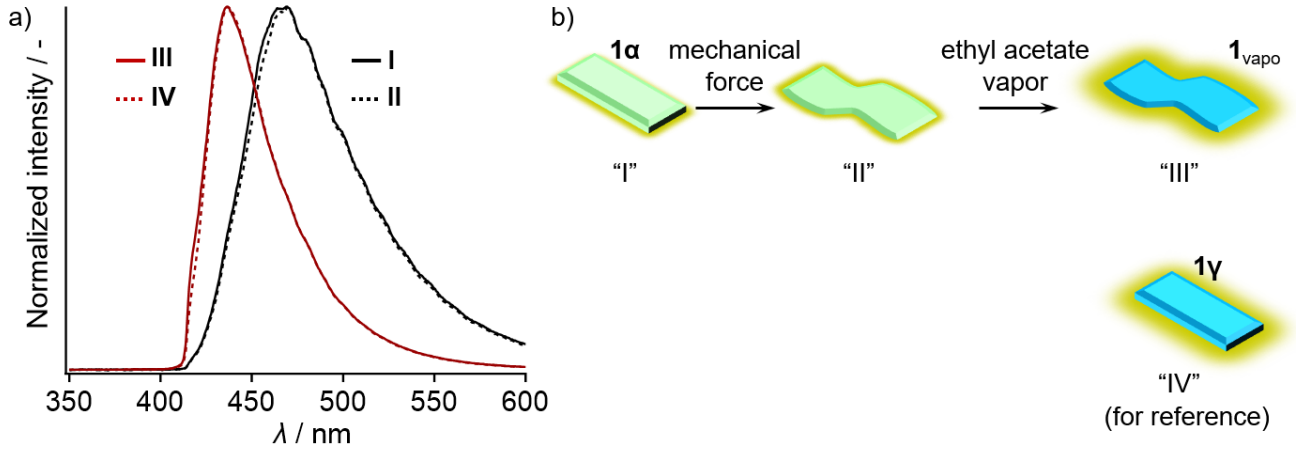

Fig. S21 a) Luminescence microscopic spectra of **1α** ("I", black solid line), bent **1α** ("II", black dotted line), bent $\mathbf{1}_{vapo}$ ("III", red solid line), and **1γ** ("IV", red dotted line) under excitation at 365 nm. b) Schematic representation for this experiment.

8. Waveguide activities

Waveguide experiments: Spatially-resolved μ-PL spectra were measured by an analyzing system [405 nm UV laser OptoSigma LDU33-405-3.5 (Sigma-Koki), micro-PL spectra using a USB400 and a R200-7-UV-VIS probe] recorded by a CCD (detector: Sony ILX511B linear silicon CCD array). The excitation laser was filtered with a band-pass filter (YIF-BA460IFS) and focused on the crystal samples with an objective (×50, NA = 0.80 or ×20, NA = 0.45). The crystal samples were excited at 5.0 μW. The collected PL was then guided to a spectrometer (Lambda Vision SA-100 A) and recorded by a CCD (detector: Hamamatsu photonics S11151-2048 CCD linear image sensor). The system is illustrated below.

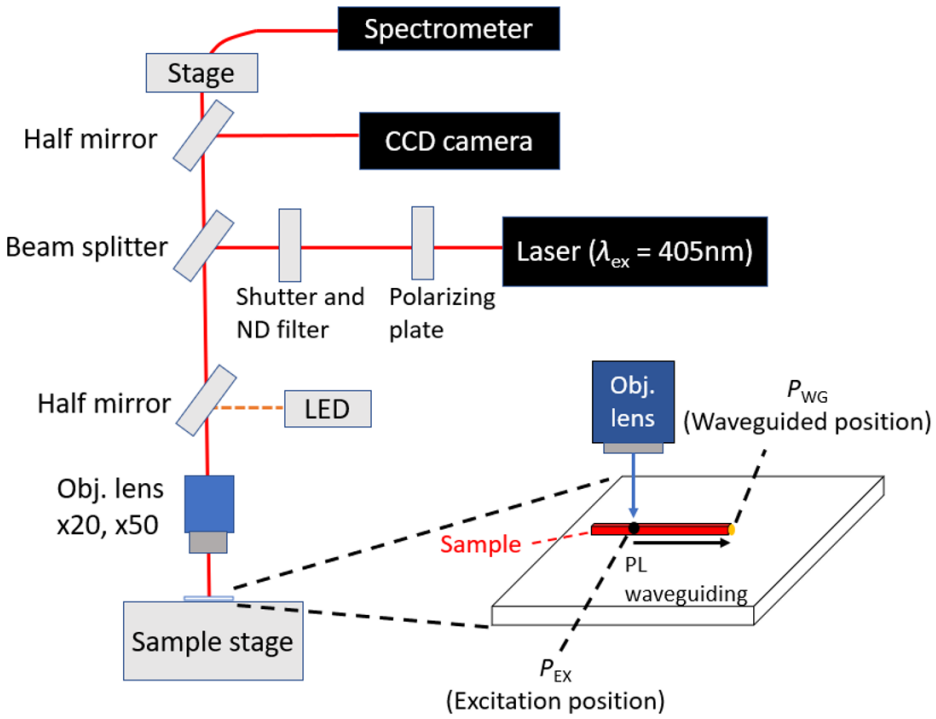

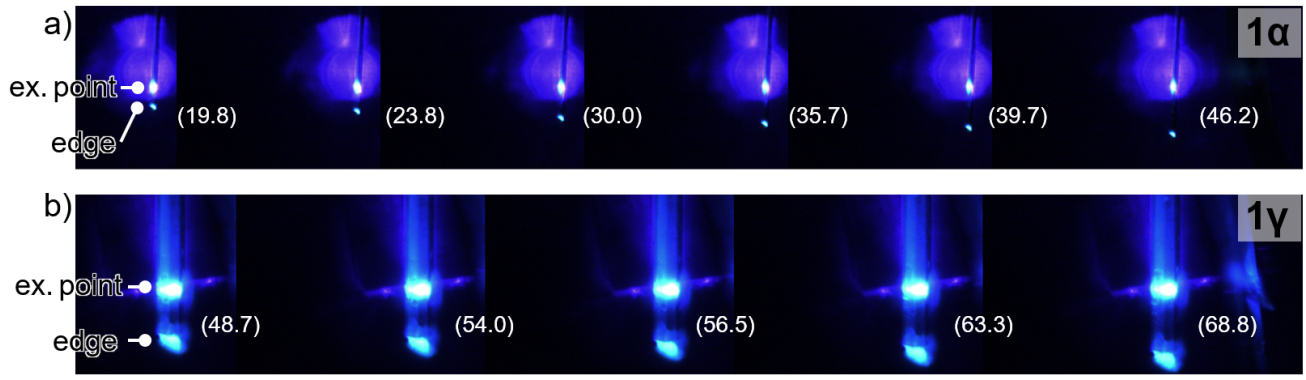

Fig. S22 a) Fluorescence images of a) pristine **1α** and b) pristine **1γ** with laser excitation (λ_{ex} = 405 nm) applied at different positions along the long-axis direction. The distance between the excitation and detection points (D in μm) is denoted in parentheses. The same images are shown in Fig. 8a and 8b in the main text.

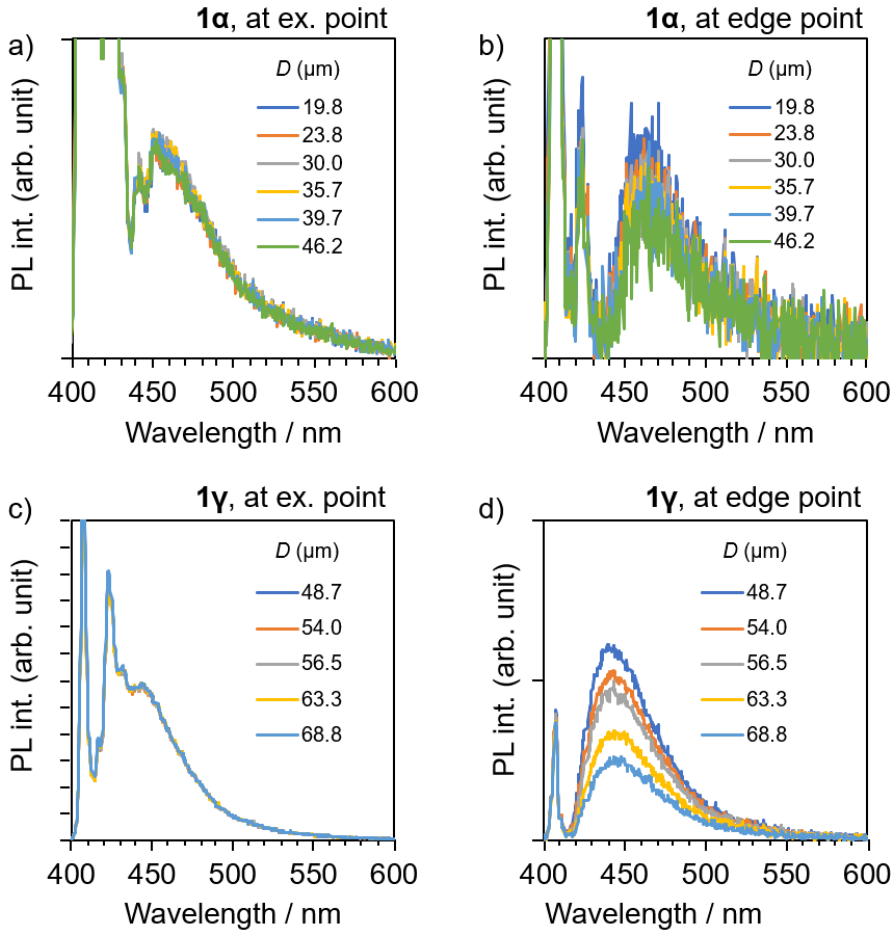

Fig. S23 The spatially resolved μ-PL spectra measured at the excitation and the edge positions of a,b) **1α** and c,d) **1γ**.

Note: The small spikes probably derived from unavoidable cosmic ray or the sensor noises of the CCD detector.

9. References

[S1] G. M. Sheldrick, SHTLXT - Integrated space-group and crystal-structure determination. *Acta Cryst.* **2015**, *A71*, 3–8.

[S2] G. M. Sheldrick, Crystal structure refinement with SHELXL. *Acta Cryst.* **2015**, C*71,* 3–8.

[S3] [1] O. V. Dolomanov, L. J. Bourhis, R. J. Gildea, J. A. Howard, H. Puschmann, OLEX2: a complete structure solution, refinement and analysis program. *J. Appl. Crystallogr.* **2009**, *42,* 339–341.

[S4] C. F. Macrae, I. Sovago, S. J. Cottrell, P. T. Galek, P. McCabe, E. Pidcock, M. Platings, G. P. Shields, J. S. Stevens, M. Towler, Mercury 4.0: from visualization to analysis, design and prediction. *J. Appl. Crystallogr.* **2020***, 53*, 226–235.

[S5] L. Waterloo, H. Hubner, F. Fierro, T. Pfeiffer, R. Brox, S. Lober, D. Weikert, M. Y. Niv, P. Gmeiner, Discovery of 2-Aminopyrimidines as Potent Agonists for the Bitter Taste Receptor TAS2R14. *J. Med. Chem.,* **2023**, *66*, 3499–3521.

[S6] Gaussian 09, Revision C.01, M. J. Frisch, G. W. Trucks, H. B. Schlegel, G. E. Scuseria, M. A. Robb, J. R. Cheeseman, G. Scalmani, V. Barone, B. Mennucci, G. A. Petersson, H. Nakatsuji, M. Caricato, X. Li, H. P. Hratchian, A. F. Izmaylov, J. Bloino, G. Zheng, J. L. Sonnenberg, M. Hada, M. Ehara, K. Toyota, R. Fukuda, J. Hasegawa, M. Ishida, T. Nakajima, Y. Honda, O. Kitao, H. Nakai, T. Vreven, J. A. Montgomery, Jr., J. E. Peralta, F. Ogliaro, M. Bearpark, J. J. Heyd, E. Brothers, K. N. Kudin, V. N. Staroverov, R. Kobayashi, J. Normand, K. Raghavachari, A. Rendell, J. C. Burant, S. S. Iyengar, J. Tomasi, M. Cossi, N. Rega, J. M. Millam, M. Klene, J. E. Knox, J. B. Cross, V. Bakken, C. Adamo, J. Jaramillo, R. Gomperts, R. E. Stratmann, O. Yazyev, A. J. Austin, R. Cammi, C. Pomelli, J. W. Ochterski, R. L. Martin, K. Morokuma, V. G. Zakrzewski, G. A. Voth, P. Salvador, J. J. Dannenberg, S. Dapprich, A. D. Daniels, Ö. Farkas, J. B. Foresman, J. V. Ortiz, J. Cioslowski, and D. J. Fox, Gaussian, Inc., Wallingford CT, 2009.

[S7] Spartan ’20; Wavefunction, Inc.: Irvine, CA.

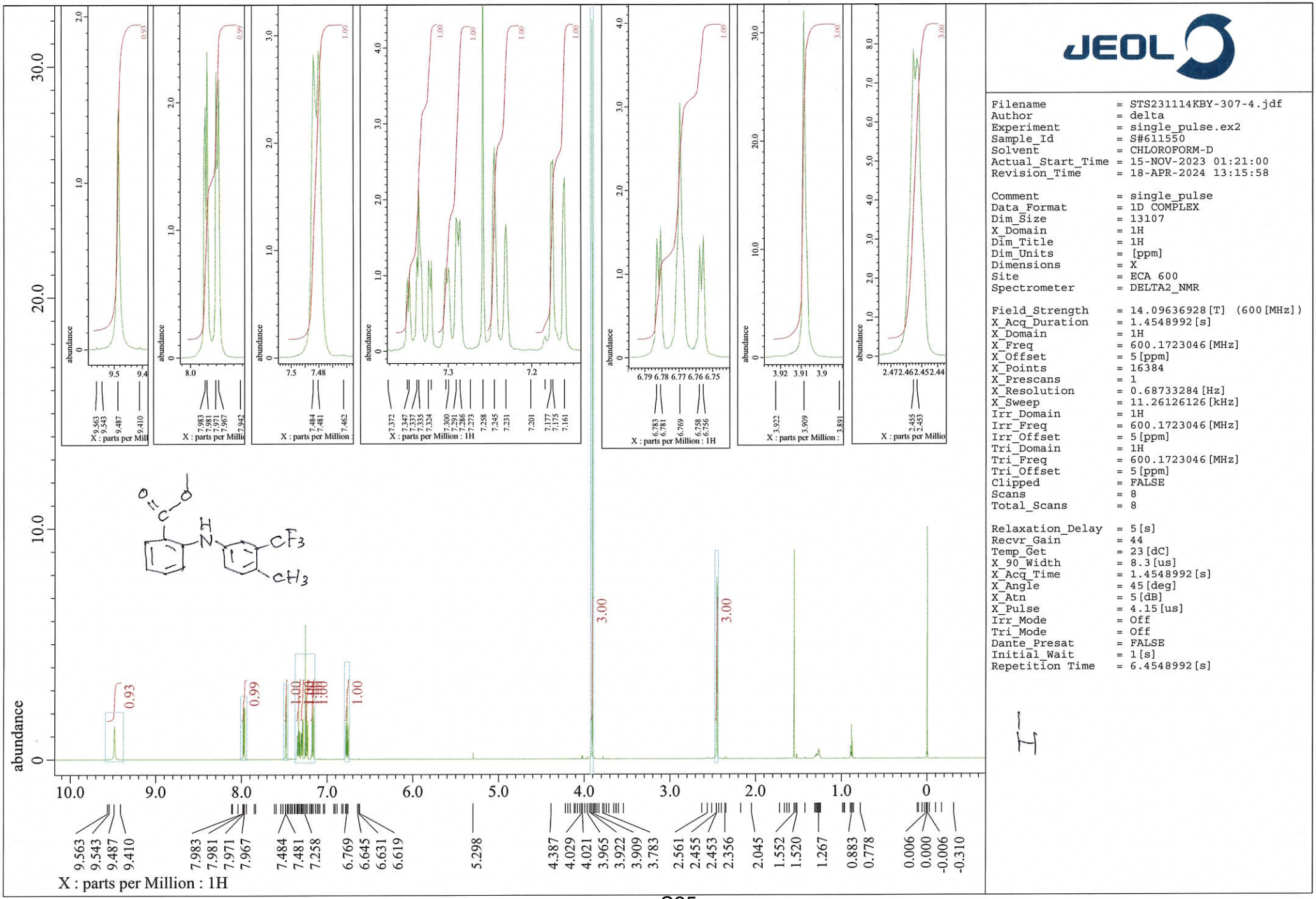

JEOL

Filename	= STS231114KBY-307-4.jdf
Author	= delta
Experiment	= single_pulse.ex2
Sample_Id	= S#611550
Solvent	= CHLOROFORM-D
Actual_Start_Time	= 15-NOV-2023 01:21:00
Revision_Time	= 18-APR-2024 13:15:58
Comment	= single_pulse
Data_Format	= 1D COMPLEX
Dim_Size	= 13107
X_Domain	= 1H
Dim_Title	= 1H
Dim_Units	= [ppm]
Dimensions	= X
Site	= ECA 600
Spectrometer	= DELTA2_NMR
Field_Strength	= 14.09636928[T] (600[MHz])
X_Acq_Duration	= 1.4548992[s]
X_Domain	= 1H
X_Freq	= 600.1723046[MHz]
X_Offset	= 5[ppm]
X_Points	= 16384
X_Prescans	= 1
X_Resolution	= 0.68733284[Hz]
X_Sweep	= 11.26126126[kHz]
Irr_Domain	= 1H
Irr_Freq	= 600.1723046[MHz]
Irr_Offset	= 5[ppm]
Tri_Domain	= 1H
Tri_Freq	= 600.1723046[MHz]
Tri_Offset	= 5[ppm]
Clipped	= FALSE
Scans	= 8
Total_Scans	= 8
Relaxation_Delay	= 5[s]
Recvr_Gain	= 44
Temp_Get	= 23[dC]
X_90_Width	= 8.3[us]
X_Acq_Time	= 1.4548992[s]
X_Angle	= 45[deg]
X_Atn	= 5[dB]
X_Pulse	= 4.15[us]
Irr_Mode	= Off
Tri_Mode	= Off
Dante_Presat	= FALSE
Initial_Wait	= 1[s]
Repetition Time	= 6.4548992[s]

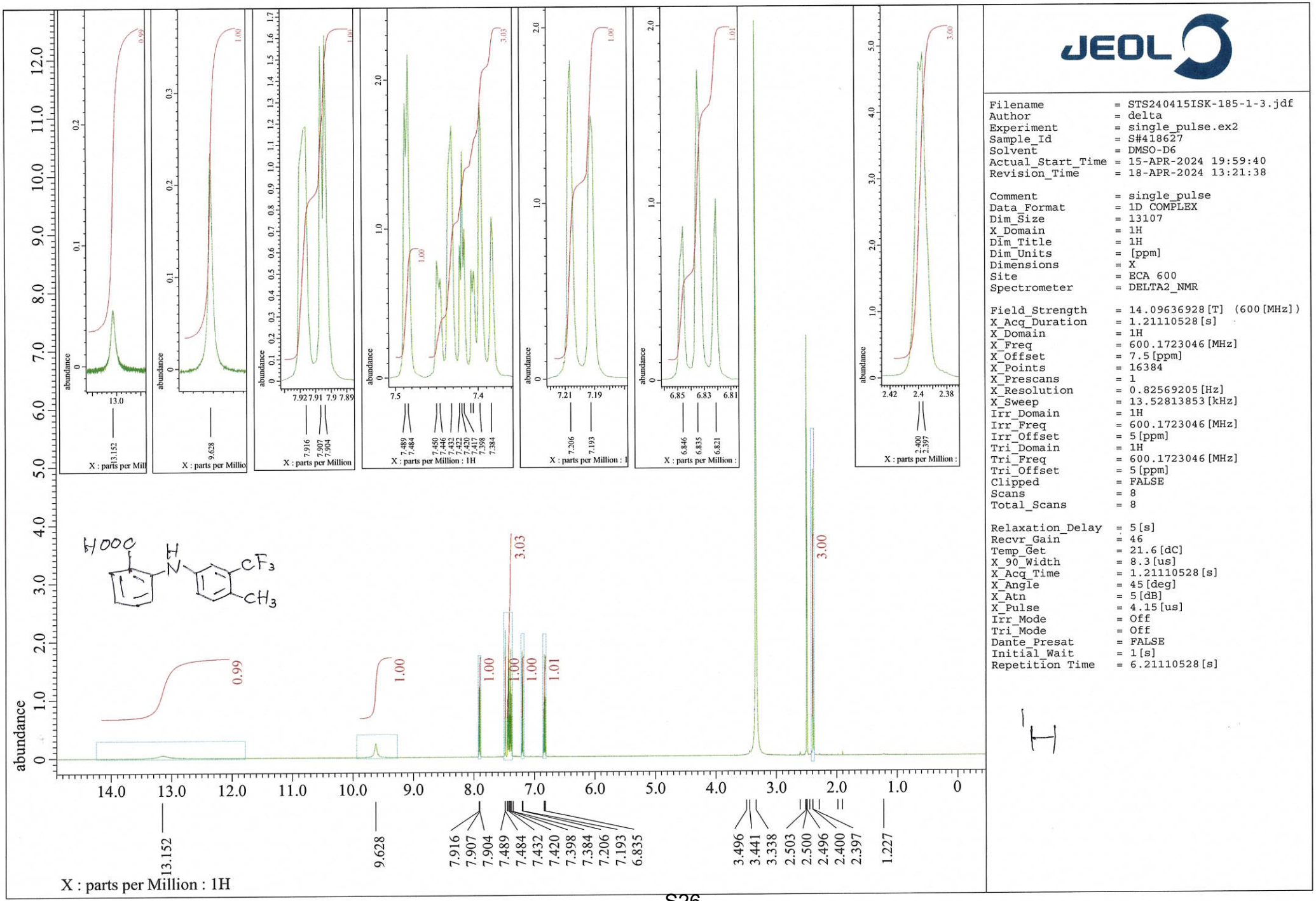

JEOL

Filename	= STS240415ISK-185-1-3.jdf
Author	= delta
Experiment	= single_pulse.ex2
Sample_Id	= S#418627
Solvent	= DMSO-D6
Actual_Start_Time	= 15-APR-2024 19:59:40
Revision_Time	= 18-APR-2024 13:21:38
Comment	= single_pulse
Data_Format	= 1D COMPLEX
Dim_Size	= 13107
X_Domain	= 1H
Dim_Title	= 1H
Dim_Units	= [ppm]
Dimensions	= X
Site	= ECA 600
Spectrometer	= DELTA2_NMR
Field_Strength	= 14.09636928[T] (600[MHz])
X_Acq_Duration	= 1.21110528[s]
X_Domain	= 1H
X_Freq	= 600.1723046[MHz]
X_Offset	= 7.5[ppm]
X_Points	= 16384
X_Prescans	= 1
X_Resolution	= 0.82569205[Hz]
X_Sweep	= 13.52813853[kHz]
Irr_Domain	= 1H
Irr_Freq	= 600.1723046[MHz]
Irr_Offset	= 5[ppm]
Tri_Domain	= 1H
Tri_Freq	= 600.1723046[MHz]
Tri_Offset	= 5[ppm]
Clipped	= FALSE
Scans	= 8
Total_Scans	= 8
Relaxation_Delay	= 5[s]
Recvr_Gain	= 46
Temp_Get	= 21.6[dC]
X_90_Width	= 8.3[us]
X_Acq_Time	= 1.21110528[s]
X_Angle	= 45[deg]
X_Atn	= 5[dB]
X_Pulse	= 4.15[us]
Irr_Mode	= Off
Tri_Mode	= Off
Dante_Presat	= FALSE
Initial_Wait	= 1[s]
Repetition Time	= 6.21110528[s]

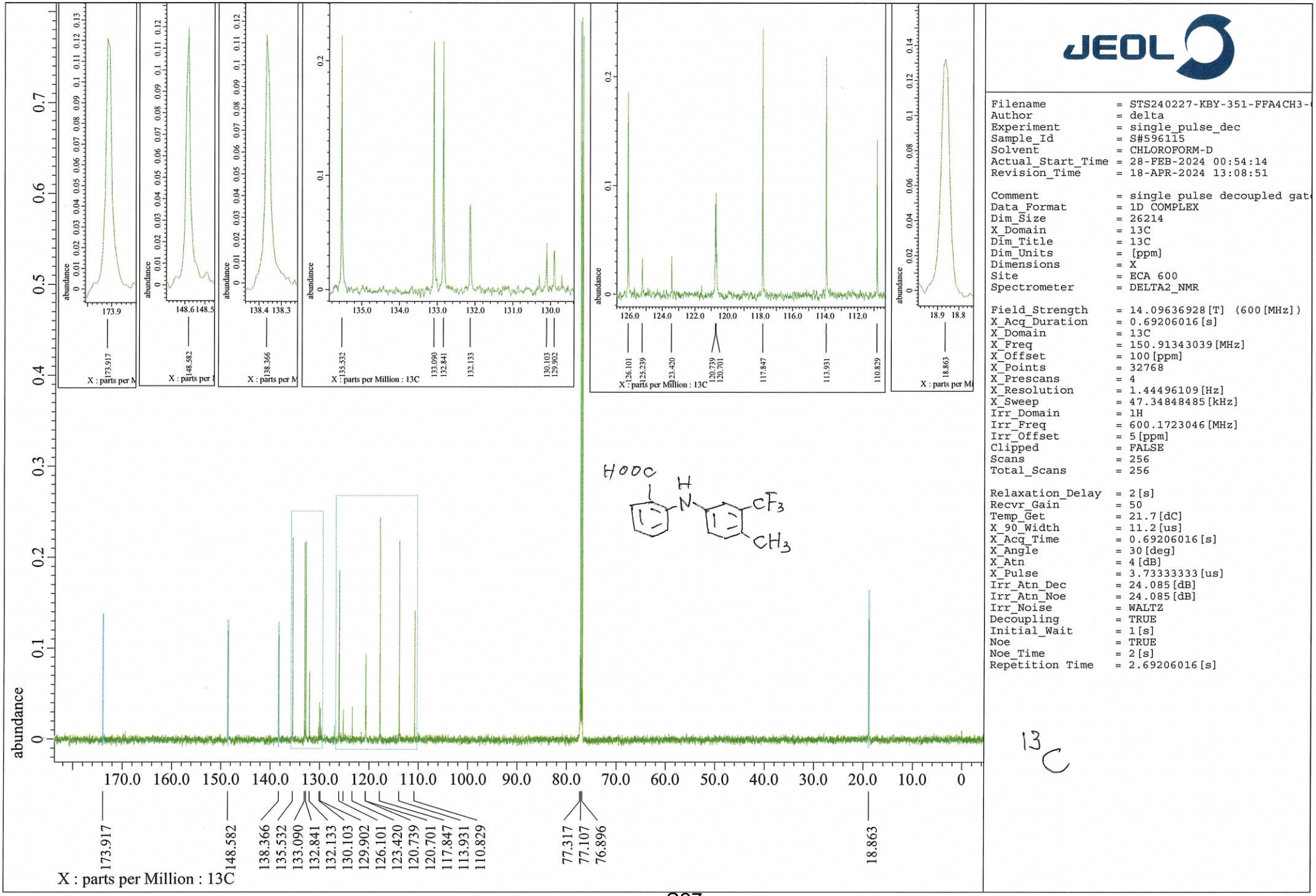
JEOL
Filename = STS240227-KBY-351-FFA4CH3-
Author = delta
Experiment = single_pulse_dec
Sample_Id = S#596115
Solvent = CHLOROFORM-D
Actual_Start_Time = 28-FEB-2024 00:54:14
Revision_Time = 18-APR-2024 13:08:51
Comment = single pulse decoupled gat
Data_Format = 1D COMPLEX
Dim_Size = 26214
X_Domain = 13C
Dim_Title = 13C
Dim_Units = [ppm]
Dimensions = X
Site = ECA 600
Spectrometer = DELTA2_NMR
Field_Strength = 14.09636928[T] (600[MHz])
X_Acq_Duration = 0.69206016[s]
X_Domain = 13C
X_Freq = 150.91343039[MHz]
X_Offset = 100[ppm]
X_Points = 32768
X_Prescans = 4
X_Resolution = 1.44496109[Hz]
X_Sweep = 47.34848485[kHz]
Irr_Domain = 1H
Irr_Freq = 600.1723046[MHz]
Irr_Offset = 5[ppm]
Clipped = FALSE
Scans = 256
Total_Scans = 256
Relaxation_Delay = 2[s]
Recvr_Gain = 50
Temp_Get = 21.7[dC]
X_90_Width = 11.2[us]
X_Acq_Time = 0.69206016[s]
X_Angle = 30[deg]
X_Atn = 4[dB]
X_Pulse = 3.73333333[us]
Irr_Atn_Dec = 24.085[dB]
Irr_Atn_Noe = 24.085[dB]
Irr_Noise = WALTZ
Decoupling = TRUE
Initial_Wait = 1[s]
Noe = TRUE
Noe_Time = 2[s]
Repetition Time = 2.69206016[s]
HOOC
CF3
CH3
13C
abundance
X : parts per Million : 13C
173.917
148.582
138.366
135.532
133.090
132.841
132.133
130.103
129.902
126.101
123.420
120.739
120.701
117.847
113.931
110.829
77.317
77.107
76.896
18.863

C:\Users\...\240402_seki\240402_seki_02 2024/04/02 11:29:50